The Design by Molecular Dynamics Modeling and Simulations of Porous Polymer Adsorbent Media Immobilized on the Throughpore Surfaces of Polymeric Monoliths

E. Riccardi, J.-C. Wang, and **A.I. Liapis***

Department of Chemical and Biological Engineering, Missouri University of Science and Technology, 400 West 11th Street, Rolla, Missouri 65409-123

Abstract

Ion-exchange porous adsorbent media having intermediate and low surface densities of dextran polymer grafted on the surface of the throughpores of polymeric monoliths are constructed and characterized by a molecular dynamics modeling and simulation approach that has also been shown to be effective in the construction and characterization of porous ion-exchange adsorbent media whose number of immobilized dextran polymer chains per unit surface area is high. The activation step that prepares the surface of the pores of the dextran polymer layer for the immobilization of the charged ligands insignificantly affected the pore structure of the dextran polymer layer, while this was found to not be the case for previously studied systems that involved high dextran polymer surface densities. Compared to the high dextran polymer density system studied previously, the intermediate dextran polymer density system can generate significantly larger pores but still possesses relatively high interconnection and mutual steric support between dextran chains to exhibit similar structural characteristics and responses to charged ligand immobilization, including dextran layer thickness, stability, monomer distribution, ligand-induced compact chain structures, dextran layer shrinkage, distributions of ligands and counterions, and local nonelectroneutrality. The low dextran polymer density system having relatively isolated dextran chains and insufficient mutual steric support can result in even larger pores than those obtained in the intermediate dextran polymer density system, but a significantly thinner porous dextran polymer layer and different dextran monomer distributions are obtained in the low dextran polymer density system. More importantly, the gradient of the local nonelectroneutrality after the immobilization of the charged ligands is significantly smaller in magnitude in the low dextran polymer density system than that obtained in the system having intermediate dextran polymer density, and, despite a lack of porous layer depth to accommodate adsorbate biomolecules in large amounts, it could still be useful for the effective transport and adsorption of very large biomolecules. Compared with the polymeric monoliths without a porous dextran polymer layer grafted on the surface of their throughpores, the intermediate and low dextran polymer density systems explored and studied in this work provide pore structures with desirable characteristics for the effective transport of adsorbate biomolecules and substantially larger effective surface areas and throughput capacities for the adsorption of the adsorbate biomolecules.

* Author to whom correspondence should be addressed: email ail@mst.edu.

Introduction

The polymeric monoliths exhibit less organized morphological features than the inorganic monoliths (1), and their features are formed by clustered microglobules. The microglobules are nonporous and the surface area of the polymeric monoliths rarely exceeds 10 m^2/g (1,2). In the pores of the polymeric monoliths, bulk fluid flow occurs, and these pores are called throughpores (2,3). Experimental data show that the polymeric monoliths provide excellent separation of large molecules like peptides, hormones, and proteins, while this is not the case for the silica-based monoliths (1). But the low surface areas of the polymeric monoliths indicate that their capacity for adsorption is rather low. The magnitude of this problem can be reduced by grafting (4–12) onto the surface of the throughpores extender polymers (e.g., dextran polymer chains), which form a porous polymer structure due to the interaction of the polymer chains. On the surface of the pores of the grafted polymer structure, the desired affinity groups/ligands can then be attached in order to form an adsorbent medium that can be used to effectively separate a species of interest from a mixture of biomolecules (4–12).

The thickness of the grafted porous polymer layer along the direction that is normal to the surface of a throughpore, the size of the pores, the pore-size distribution, the pore connectivity, the distribution of the pore connectivity, the pore

volume, and the pore surface area of the grafted polymer layer depend on (7,11,12) the length and the degree of side-branching of the polymer chain, the number of attachment points on the surface of the throughpores (base matrix), and the number of main polymer chains immobilized per unit surface area of base matrix (throughpores). The grafted porous polymer layer on the surface of the throughpores could significantly increase the surface area of the polymeric monoliths, and this could increase the overall number of affinity groups/ligands that could be immobilized, which in turn could increase the adsorption capacity (4,9–12), and, especially in the case of ion-exchange chromatography, could substantially increase the uptake rate (8–10,13–15). The grafted flexible (7,11,12) porous polymer layer is permeable to macromolecules and is considered to increase (2,4–7,9–12) the effective volume and the steric availability of the affinity groups/ligands for the adsorbate macromolecules to be adsorbed, and this could, in turn, increase the mass transfer rate as well as the total capacity for adsorption. It is worth mentioning here that the thickness of the grafted porous polymer layer along the direction that is normal to the surface of a throughpore could be (4,7,11,12) between 75 Å and 250 Å and depends on the variables discussed previously. The grafted porous polymer layer on the surface of the throughpores may have a very high local concentration of functionalities because it can be prepared from a neat functional monomer (11,12). On the other hand, dilution of the functional monomer with a non-functional one enables precise control of the density of functionalities (11,12). The grafting procedure could also enable the creation of a gradient of density of functionalities along the axis of the polymeric monolith, and this can result in the construction of a monolithic column with only a few functional groups at one end and many more at the opposite end (12).

In the process employed for the construction of porous polymer adsorbent media (4–7,11,12), stage I is considered to concern itself with the construction of the porous polymer layers formed from the mutual interaction of the polymeric extender molecules which are grafted on the surface of the pores of the base matrix, while stage II involves the immobilization of the affinity groups/ligands on the surface of the pores of the immobilized porous polymer layers. The adsorption process of the charged biomolecules of interest onto the affinity groups/ligands is considered to represent stage III in the study of the separation of biomolecules by ion-exchange adsorption, employing polymeric adsorbent particles whose formation involves stages I and II. Riccardi et al. (11) presented a novel and effective approach for the construction of dextran polymer layers on agarose surfaces by a molecular dynamics (MD) modeling and simulation method. As long as the sizes of the desired affinity group/ligand to be immobilized and of the desired charged biomolecule (adsorbate) to be separated by ion-exchange adsorption are known, then the work of Riccardi et al. (11) can be used to design and construct in stage I porous polymer structures having desirable characteristics with respect to pore size, pore size distribution, pore connectivity, and pore connectivity distribution which represent key measures for the characterization of a porous structure. Furthermore, Riccardi et al. (11) also presented a methodology by which the most desirable porous polymer structure from a set of constructed porous polymer structures could be selected, for a given affinity group/ligand and a charged adsorbate biomolecule desired to be separated. Also, Riccardi et al. (12) constructed and presented an MD modeling and simulation approach for the immobilization of charged ligands on the surface of porous dextran polymer layers in order to study stage II. It is important to mention here that the modeling and simulation approach, as well as the methods of analysis of pore structures, presented by Riccardi et al. (11,12) can also be used when (*i*) the base matrix is made from a polymer other than agarose and (*ii*) the grafted porous layer is made from polymer chains other than dextran, as long as the potential energy models employed in the modeling and simulation methods presented by Riccardi et al. (11,12) account properly for the polymeric material that the surface of the pores of the base matrix is made from, and for the kind of polymer chains that are grafted on the surface of the pores of the base matrix.

In this work, the MD modeling and simulation approach developed by Riccardi et al. (11,12) is employed in (*i*) the construction of porous dextran polymer layers grafted on the surface of the throughpores of a base matrix made by agarose; and (*ii*) the functionalization of the porous dextran polymer layers through the immobilization of desired affinity groups/ligands, so that the resulting porous polymer adsorbent media have desirable transport and adsorption properties for the separation of a polypeptide or protein of interest from a mixture of species. In effect, the work presented here concerns itself with stages I and II of the process employed in the construction of porous polymer adsorbent media discussed previously.

Simulation Models and Methods

Our prior works (11,12) have successfully employed the MD technique and developed a modeling and simulation methodology to generate model porous structures of polymeric dextran chains grafted on agarose surfaces that are similar to the porous structures of the adsorbent media constructed for effective ion-exchange adsorption in practice. In this work, the surface of the throughpores of the monolith is considered to be formed from agarose and on the surface of the throughpores, dextran porous polymer layers are grafted. Therefore, our previous modeling and simulation approach (11,12) can be readily applied here. Because the details of the simulation formulation and methodology have been described previously (11,12), only a brief review is given here. The surface of the throughpores of a monolithic base matrix is considered to have curved geometry and is represented by the following trigonometric surface model (11,12):

$$U_{is}(x,y,z) = 2\pi\varepsilon_{is}\left(\frac{\sigma_{is}}{R_{Os}}\right)^2\left[\frac{2}{5}\left(\frac{\sigma_{is}}{z_s}\right)^{10} - \left(\frac{\sigma_{is}}{z_s}\right)^4 - \frac{\sqrt{2}}{3\left(\frac{R_{Os}}{\sigma_{is}}\right)\left(\frac{z_s}{\sigma_{is}} + \frac{0.61}{\sqrt{2}}\frac{R_{Os}}{\sigma_{is}}\right)^3}\right] \quad \text{Eq. 1A}$$

$$z_s = z - a\left[2 + \cos\left(\frac{2\pi}{b}x\right) + \cos\left(\frac{2\pi}{b}y\right)\right] \qquad \text{Eq. 1B}$$

where U_{is} is the interaction potential energy between the base matrix and a particle i at (x,y,z) whose size and interaction strength are denoted by σ_i and ε_i. The interaction parameters are determined by the mixing rules, $\sigma_{is} = \frac{1}{2}(\sigma_i + R_{Os})$ and $\varepsilon_{is} = \sqrt{\varepsilon_i \varepsilon_{Os}}$, where R_{0s} represents the nearest distance between agarose monomers, which is taken to be the same as the diameter of a dextran monomer, and $\varepsilon_{0s} = \max(\varepsilon_{B1}, \varepsilon_{B4}, \varepsilon_{B6})$ is the interaction strength between agarose monomers. The values of a, b, R_{0s}, and ε_{0s} used in this work are the same as in our previous studies (11,12), which generate trigonometrically effective surface areas that are larger than the flat surfaces with the same linear dimensions by a factor of 1.528. The periodic boundary conditions are applied in the lateral x and y directions.

To examine the influence of dextran surface density, two cases with lower dextran density than the system employed in our previous work (11,12) are considered. The first case has 20 dextran chains on a surface with linear dimensions of 202 Å × 202 Å, resulting in an intermediate dextran polymer density that is approximately ½ of the dextran surface density considered in our previous (12) work. The second case has 10 dextran chains on a surface with linear dimensions of 404 Å × 404 Å, resulting in a low dextran polymer density that is approximately $^1/_{16}$ of the dextran surface density in our previous (12) work. The dextran polymer chains have 40 glucose monomers per main chain and 5% of side-branching, and their first monomers are immobilized at random surface locations with random rotation around their long molecular axes. They are simulated with a modified M3B model (12) where three beads denoted as B1, B4, and B6 corresponding to the C1, C4, and C6 carbons are used to represent each glucose monomer. Between the M3B beads, the bending and torsional motions are treated with $U_b(\theta) = \frac{1}{2}K_\theta(\theta_i - \theta_0)^2$ and:

$$U_{tor}(\phi) = \sum_{j=1}^{3} \frac{1}{2} B_j[1 + \cos(j\phi - \phi^0_j)]$$

for proper conformational representation and the bond lengths are constrained by the SHAKE algorithm (16). The dextran chains and the monolith surface are completely immersed in a water phase that contains 120,000 molecules in the intermediate dextran polymer density system and 480,000 water molecules in the low dextran polymer density system. The water molecules are simulated by the coarse-grain water model developed together with M3B (11,12,17).

Numerous realizations of the pore structures have been obtained with different sets of random dextran immobilization locations for each of the two cases, and their average pore-size distributions have been analyzed. Because the larger pores in the upper regions of the porous dextran polymer layers represent the practical operational channels of interest for adsorbate transport and adsorption, we use them as the criteria to select the most representative systems for further activation and ligand attachment. The selected systems are first equilibrated over a period of 0.8 ns and then activated by increasing the size of every dextran B4 bead by 3 Å to represent a uniform monolayer distribution and excluded volume effect of the activator molecules. The activated systems are re-equilibrated for another 0.5 ns.

To complete the construction of the monolithic adsorbing media, ligands and counterions have to be introduced into the equilibrated activated systems. In this work, we consider ligands to carry –e charge and to be always accompanied by the same number of counterions carrying +e charge, so that the systems maintain overall electroneutrality throughout the course of simulations. The ligands and counterions are also simulated with proper coarse grain models (11,12) and, in addition to their charge–charge interactions, they have interactions with each other and with water and dextran beads that are treated to be characteristic of polar interactions (12). It is important to emphasize here that the purpose of the ligand-attaching step is to obtain an initial ligand distribution with no intention to evaluate the mass transfer rate of the ligands or counterions into the porous media. At the start of ligand attachment, 150 ligands and 150 counterions are randomly placed above the dextran layer and given random vectorial velocities sampled from the equilibrium speed distributions at the system temperature with the perpendicular components pointing downwards, while the dextran chains are kept frozen and the water phase is temporarily modeled as a dielectric continuum (12,18). The bonding interaction between the ligands and the activated B4 sites is modeled by the same approach as for case A in our previous work (12), where a Morse potential with an interaction strength of 1.34 kcal/mol is used and the ligand-activator bond is considered to be irreversibly formed and computationally constrained by the SHAKE algorithm when a ligand molecule comes within a distance of 13.45 Å from a vacant activated B4 site. Once a ligand molecule is attached, a new one and its accompanying counterion are added randomly to the aqueous film that covers the dextran layer. In the case of the low dextran polymer density system, when multiples of 10 ligands have been attached on the dextran polymer chains, a new re-equilibration step starts for 0.2 ns, where the unattached ligands are removed from the system; the dextran chains are unfrozen, and the treatment of the water phase is switched back to the explicit model. In the case of the intermediate dextran polymer density system whose porous dextran structure has better stability, ligand immobilization is undertaken by multiples of 30 ligands coupled with a longer re-equilibration step over 0.4 ns for computational efficiency.

The MD simulations in this work are carried out using the leap-frog integration algorithm together with a Gaussian thermostat method for temperature control. During every equilibration step, the systems are first annealed to 353 K and then brought back to 298 K, and the integration time step starts out with 0.1 fs and gradually increases to 6 fs. For the results reported here, the total duration of simulation time exceeds at least 4 ns. To handle our large simulation systems, we resort to parallel computing using MPI and a 64-bit Linux-based computer that has 8 cores, each clocked at 2.4 GHz. We developed and employed our own parallel MD simulation code

for this work, which runs at a computational speed of approximately 0.3 ns/day on the Linux computer for the intermediate dextran density system with approximately 500,000 particles.

Results and Discussion

To obtain the most representative realizations for the two systems with different dextran polymer densities immobilized on the agarose surface (it is worth mentioning again here that the dextran polymer density refers to the number of dextran polymer chains that are immobilized per unit surface area of agarose), the MD simulations considered in this work have followed the methodology developed in our previous work (11,12) that puts emphasis on the construction of dextran polymer porous layers having large pore radii, so that the size of the pores can efficiently facilitate the transport and adsorption of desirables for separation biomolecules. The porous base matrices (i.e., porous agarose matrices) are activated first before ligands start to be immobilized onto the dextran chains (11, 12). Unlike the high dextran polymer density system studied and reported previously (12), the activation of the dextran polymer chains by activator molecules insignificantly affects the structural properties of the porous dextran polymer layers resulting from the interaction of the polymer chains employed in the intermediate and low dextran polymer density systems studied here. When 735 ligands have been immobilized in the system with intermediate dextran density, and 380 ligands have been immobilized in the system with low dextran density, the ligand loading reaches 0.85 and 0.88 ligands per dextran monomer, respectively, and it becomes very difficult to immobilize additional ligands. The same difficulty also arose in the previously studied high dextran density system (12) with a similar ligand loading per dextran monomer. To facilitate comparison and discussion, the results for the system with intermediate dextran density are presented in Figures 1 and 2, and for the system with low dextran density are presented in Figures 3 and 4, where the structural properties of the porous dextran layers are characterized by the distributions of the B4 beads (A), number of pore openings (B), and pore volume as a function of distance from $z = 0$ (C), which represents the position of the lowest points located on the curved agarose surfaces, to the outermost regions of the porous dextran layers.

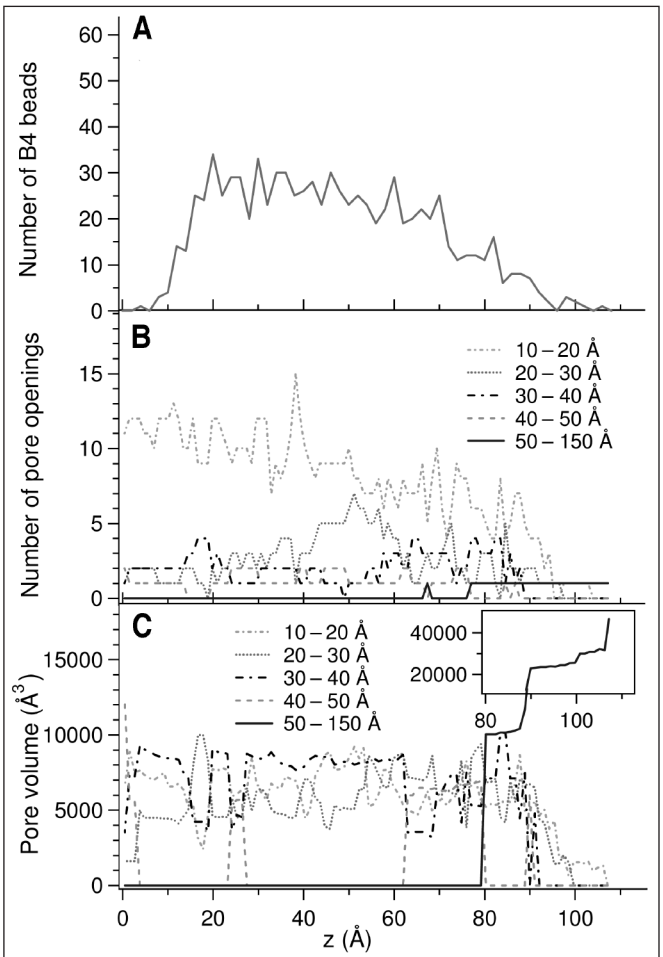

Figure 1. System of intermediate dextran polymer density: characterization of the porous dextran polymer layer before the immobilization of ligands by the distributions of the number of B4 beads (A), number of pore openings (B), and pore volume along the z direction that is perpendicular to the surface of the throughpores (C).

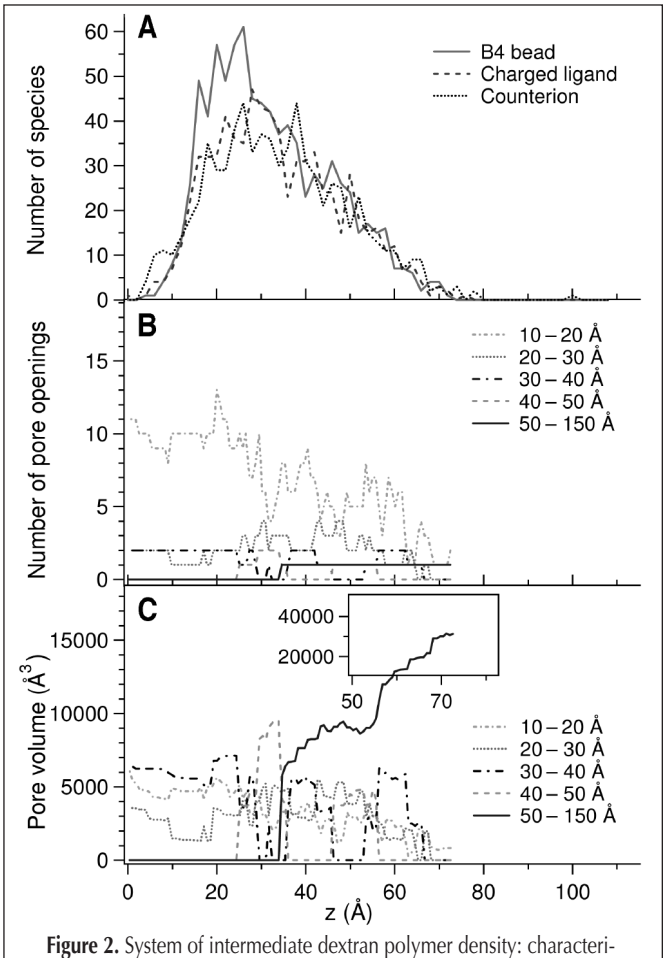

Figure 2. System of intermediate dextran polymer density: characterization of the porous dextran polymer layer after the immobilization of 735 charged ligands by the distributions of the number of B4 beads (A), charged ligands, and counterions, number of pore openings (B), and pore volume along the z direction that is perpendicular to the surface of the throughpores (C).

The method employed for such analyses has been explained in our previous work (11), except that the possibility of having cases where the pore diameters could be larger than the dextran layer thickness calls for a change of probe from spheres to cylindrical disks with a thickness of 1.85 Å that is equivalent to the average radius of the M3B beads. The top-down and inside side views of the two different dextran polymer density cases are also shown together in Figures 5 and 6 (See Pages 8A), respectively, for added visual clarification.

The data in Figure 1A suggest that the porous dextran layer of the intermediate dextran density system appears to have approximately similar average thickness and quasi-uniform dextran monomer distribution along the *z* direction as those of the high dextran density (12) system whose dextran layer extends to $z \approx 108$ Å. This indicates that sufficient mutual steric support between dextran chains still exists in the intermediate dextran density system. However, a closer examination reveals that the B4 bead distribution in the intermediate dextran density system shown in Figure 1A falls off more noticeably in the upper region of the porous polymer layer where more free volume is available from a lower dextran density, when compared with the results obtained at the upper region of the porous layer formed by the high dextran density (12) system. More importantly, while the porous dextran layer of the high dextran density system (12) has only pores whose radii are smaller than 20 Å, reducing the dextran surface density by approximately 50% allows, as indicated by the results in Figures 1B and 5, much larger pores to be created, including those that are significantly greater than 50 Å in radius. The results in Figure 1B show the trends of the curves of pore openings and their connectivity with each other [pore connectivity (11,12)] along the direction of net transport which is along the z direction (the z direction is perpendicular to the surface of the throughpores), and one can observe that the large pores can maintain a fairly constant presence along the *z* direction and have sufficiently high pore connectivity between pores of different sizes so that the net transport of the ligands to be immobilized, as well as later on the transport of the adsorbate molecules of interest, can be facilitated effectively. Such a pore structure can significantly increase the effective surface area and throughput capacity and, therefore, has the potential to provide substantially more efficient separation of desired large biomolecules when compared with the degree of separation that could be realized in a monolith system whose throughpores do not have a porous polymer layer grafted on their surfaces. It also signifies the suitability of the methodology developed previously by Riccardi et al. (11,12) for the modeling and simulation studies of polymeric monoliths.

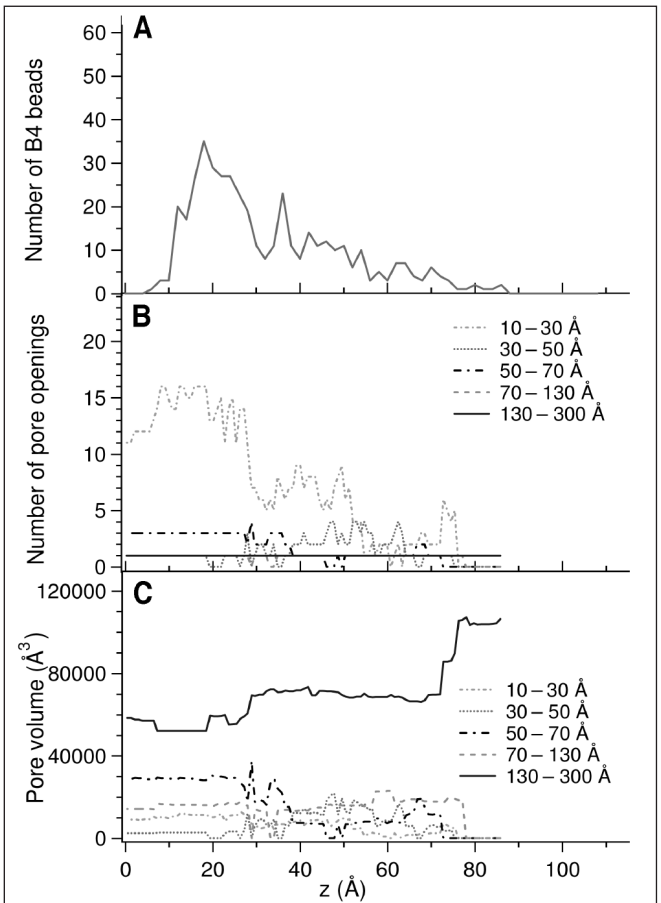

Figure 3. System of low dextran polymer density: characterization of the porous dextran polymer layer before the immobilization of ligands by the distributions of the number of B4 beads (A), number of pore openings (B), and pore volume along the *z* direction that is perpendicular to the surface of the throughpores (C).

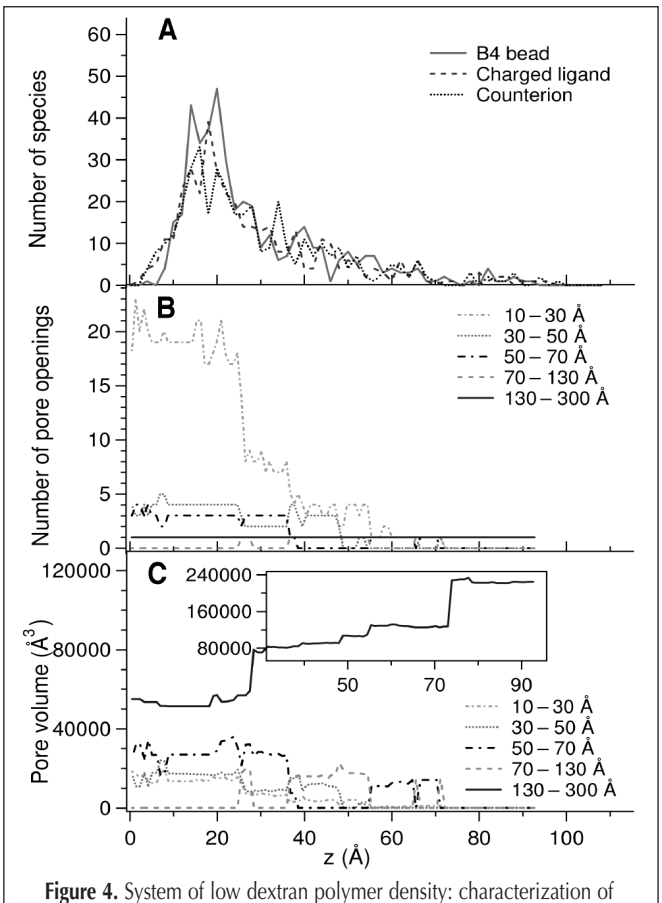

Figure 4. System of low dextran polymer density: characterization of the porous dextran polymer layer after the immobilization of 380 charged ligands by the distributions of the number of B4 beads (A), charged ligands, counterions, and number of pore openings (B), and pore volume along the *z* direction that is perpendicular to the surface of the throughpores (C).

During the early stages of the immobilization process in the intermediate dextran density system, ligands tend to be captured in the upper region of the dextran layer because the dextran chains are still relatively highly interconnected. This results in ligand distributions peaking in the upper region of the dextran layer and generating an additional energetic barrier to the subsequent ligands attempting to immobilize in the region located below the upper region of the dextran layer. The polymeric dextran layer during the early stages is a dynamic system whose structure changes continuously in response to the increasing presence of ligands and counterions. As ligand immobilization proceeds to a maximum loading, the distribution of ligands as shown in Figure 2A becomes consistent with the distribution of the B4 beads and provides a strong template to guide the distribution of counterions. Nevertheless, it is important to point out that below or above 35 Å in Figure 2A, the system equilibrated with a maximum ligand loading exhibits fewer counterions or more counterions than charged ligands, indicating a lack of local electroneutrality in the dextran layer that could have significant implications on the performance of the porous adsorbent media for adsorbing charged species (i.e., ion-exchange chromatography) and to relevant macroscopic modeling studies (2,3,5,6,8–15). Furthermore, Figures 1, 2, and 5 together also indicate that the immobilized charged ligands and the accompanying counterions increase the cohesive energy of the functionalized dextran layer with their strong coulombic interactions, thereby causing the dextran chains to form more compact conformations and configurations and more rounded shapes. Thus, the dextran layer thickness shrinks by approximately 34 Å, which is approximately 2 Å more than the ligand-induced shrinkage in the high dextran density system (12). These transitions significantly increase the difficulty for subsequent ligand immobilization but also enhance the stability of the porous structure, especially with regard to the stability of the largest pores that are of central interest in the present work. In fact, Figures 2 and 5 appear to suggest that in the shrinking dextran porous layer functionalized by ligands, small pores diminish to favor large pores to become even larger, and the good pore connectivity (11,12) from the base (see Figure 1B) dextran layer is well preserved vertically and laterally.

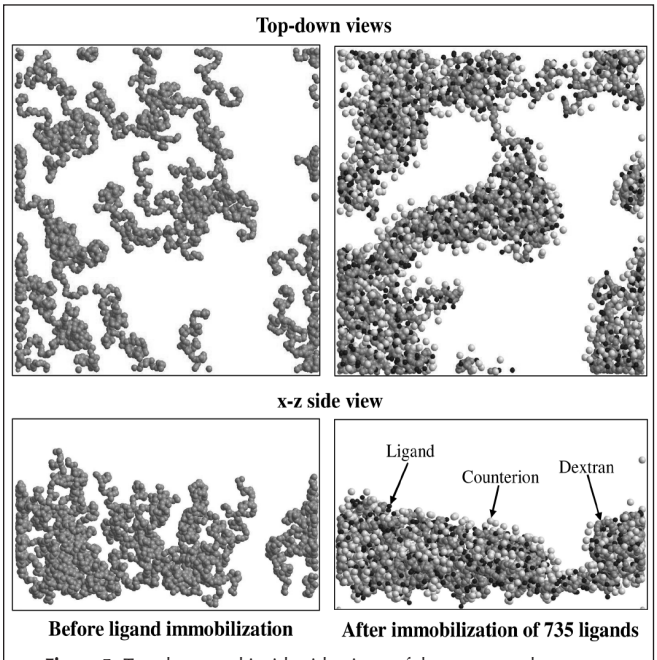

Figure 5. Top-down and inside side views of the porous polymer system having intermediate dextran polymer density and where the dextran chains, charged ligands, and counterions are represented by grey, black, and white beads, respectively.

Reducing the dextran surface density by a factor of approximately 16 makes the low dextran polymer density system studied here quite different from the high density system reported previously (12) and the intermediate density system previously discussed. The first sign of its differences is the B4 bead distribution of the base dextran layer shown in Figure 3A that is no longer quai-uniform but has a big lump below z = 32 Å with a maximum at 20 Å. Side views of simulation snapshots shown in Figure 6 show that most dextran chains have lower segments collapsing together onto the surface and some polymer chains tilt significantly, resulting in a dextran layer at least 20 Å thinner than the corresponding base dextran layers obtained in the systems having intermediate to high dextran densities. This is apparently caused by insufficient mutual steric support among dextran chains due to a wider space available (*i*) for the initial grafting of the dextran polymer chains and (*ii*) for the grafted dextran chains to have greater degrees of movement. From this point of view, it can be readily understood and also observed in Figures 3B and 6 that two big pores with average radii of 80 Å and 140 Å can be created by the low dextran surface density and can stretch from the top to the bottom of the dextran layer, while the number and volume of smaller pores in the pore radii range of 10–30 Å decrease significantly from z = 32 Å to the agarose surface.

The large in size pores and relatively isolated dextran chains in the low dextran density system provide the greatest accessibility for charged ligands onto the activated B4 sites and for

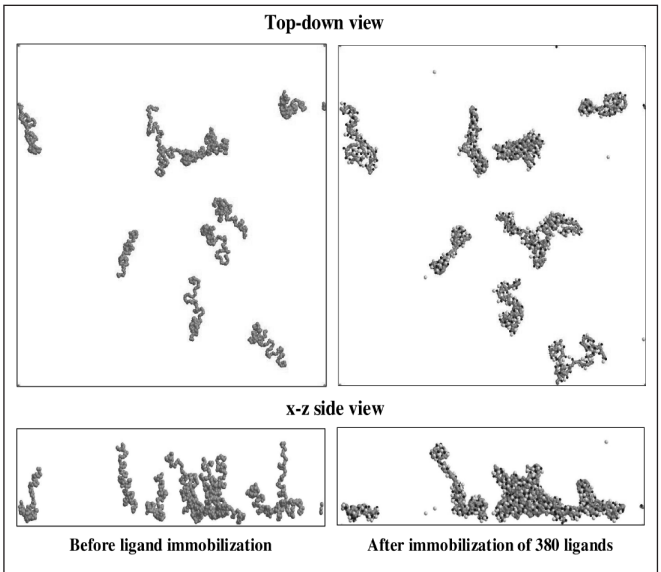

Figure 6. Top-down and inside side views of the porous polymer system having low dextran polymer density and where the dextran chains, charged ligands, and counterions are represented by grey, black, and white beads, respectively.

counterions to couple with immobilized ligands. As a result, the aforementioned structural and energetic barriers encountered during the early stages of ligand immobilization in the systems having intermediate and high dextran polymer densities are virtually nonexistent in the system having low dextran polymer density, and the distributions of immobilized ligands and accompanying counterions are consistent with the distribution of the B4 beads throughout the immobilization process, and thus, the gradient of local nonelectroneutrality is significantly smaller in this low dextran density system. As the ligand loading increases, so does the cohesive energy of dextran chains and the compactness of their chain structures. It is important to point out here that the dextran chains loaded with charged ligands and counterions in the low dextran density system almost all fold individually to form single-chain compact structures as indicated by the top-down view in Figure 6, which worsens the already insufficient mutual steric support among dextran chains to let some of them fall entirely onto the surface. However, the dextran layer thickness appears to be almost unaffected when comparing Figures 3B and 4B, because while other dextran chains fold, one stretched dextran chain is able to sustain the impact of immobilized ligands and counterions to maintain most of its height in the z direction and consequently the nominal thickness of dextran layer. Analysis of simulation snapshots reveals that this becomes possible when the dextran chain captures sufficiently more ligands than surrounding counterions to result in a net charge and repulsion within the chain molecule that keeps the dextran chain stretched. When the ligands are finally neutralized by counterions, they together form a sheath to further support the stretched structure. These structural transitions also cause the changes in the pore structure observed in Figures 3 and 4. In general, after dextran chains are induced by ligand immobilization to fold and to flatten on the surface, their cross-section areas have increased enough to narrow the second largest pore down to the smaller size range of 50–70 Å in the upper region and to completely convert the second largest pore to smaller ones, mainly in the size ranges of 10–30 Å and 30–50 Å in the region below z = 23 Å.

From the results presented previously, the appropriateness of the dextran layer in the low dextran density system appears to be questionable because its pores lack the depth along the z direction possessed by the pores in the systems with intermediate or high dextran densities to accommodate the transport and adsorption of adsorbate biomolecules. The grafted dextran polymer chains in the low density system can even be considered to just corrugate the surface, and this would appear to produce a kind of fractal surface which could still have a larger surface area and, therefore, larger adsorption capacity than those that could have been obtained when no dextran polymer chains had been grafted on the throughpore surfaces of the monolith. Thus, the low density system should not be considered a pathological case because despite having limited capacity, it can still provide useful bioseparations, especially for very large adsorbate biomolecules. The results in Figures 2 and 4 on nonelectroneutrality also suggest that the monolith surface can be modified with certain charges in advance, as was also discussed in the case of the high dextran polymer density system (12), to create a surface potential that influences the distributions of immobilized ligands and counterions and consequently the pore structure, so that the efficient transport and adsorption of the biomolecules of interest can be facilitated. Such surface modification can be taken one step further so that intentionally different surface potentials from different amounts of surface charges can be obtained in a preassigned manner to achieve better separation performance.

Conclusions

The MD modeling and simulation approach developed by Riccardi et al. (11,12) was used to build porous dextran ion-exchange adsorbent media grafted on the surface of the throughpores of polymeric monoliths (i.e., porous agarose matrices), so that the effective surface area and throughput capacity of the polymeric monoliths can be substantially increased. The characterization of the pore structures and the local nonelectroneutrality of the grafted porous dextran polymer ion-exchange adsorbent media were studied for two cases representing intermediate and low dextran polymer densities immobilized on the surface of the throughpores of the monolith.

The results indicate that the activation step which activates the surface of the pores of the dextran polymer layer so that the immobilization of ligands can be realized, had negligible impact on the pore structure of the porous dextran layer for the two cases studied in this work, while the activation step was found (12) to significantly affect the pore structure of systems having high dextran polymer densities. The immobilization of the ligands affected the pore structure of the systems studied here, as was the case (12) for the high dextran polymer density systems, but the effect of the immobilization of ligands on the pore structure was more significant in the system having a low dextran density than in the system of the intermediate dextran density. The intermediate dextran density system exhibits sufficient mutual steric support between dextran chains, as was (12) the case with the high dextran density system, while this is not the case for the low dextran density system where most dextran chains have lower segments collapsing together onto the surface of the base matrix, and this results to the formation of a porous dextran layer whose thickness along the net direction of transport, z, is substantially thinner than the thickness of the porous dextran layer obtained from the intermediate dextran density system. It is important to note here that while the structural characteristics along the net direction of transport, z, in the porous dextran layer are rather similar for the systems having high and intermediate dextran densities, there are very significant differences along the z direction between the pore structures of the intermediate and low dextran density systems. And this could be considered to suggest that the transport and adsorption behavior of the desired biomolecule might differ more substantially in the system of low dextran density when compared to that encountered in the system of intermediate dextran density, while the differences in the transport and adsorption behavior of the biomolecule in the pore structures

formed by high and intermediate dextran density systems might not be as large in magnitude as those encountered in the comparison between the low and intermediate dextran density systems. Both the intermediate and low dextran density systems form significantly larger pores than those encountered in the case of high (12) dextran density systems, and even the low density system could provide a substantially larger effective surface area and throughput capacity for adsorption than that it could have been obtained if the porous dextran polymer layer had not been grafted on the surface of the throughpores of the monolith. Therefore, the intermediate and the low dextran density systems could facilitate the effective transport and adsorption of large biomolecules, and the low dextran density system could especially be useful for the effective transport and adsorption of very large biomolecules. These results also signify the suitability of the methodology developed previously by Riccardi et al. (11,12) for the modeling and simulation studies of polymeric monoliths.

The magnitude of the gradient of the local nonelectroneutrality along the *z* direction is found to be significantly smaller in the system of low dextran density than that obtained in the intermediate dextran density system, and this could have significant implications with respect to the transport and adsorption of the desired adsorbate biomolecules. Furthermore, the differences in the magnitudes of the gradients of the local nonelectroneutrality between the low and intermediate dextran density systems are larger than those encountered between the high and intermediate dextran density systems. This finding, with respect to the local nonelectroneutrality together with the finding regarding the structural differences along the *z* direction for the systems having different dextran densities discussed in the previous paragraph, suggest that the variation in the properties of the dextran polymer ion-exchange media might be larger, and, therefore, operationally more significant with respect to pore transport and throughput capacity, between the intermediate and low dextran density systems than between the high and intermediate dextran density systems. This represents an area that is worth further research, especially if one would like to ascertain the effect of having different spatial density distributions of ligands so that a gradient of density of functionalities along the axis of liquid bulk flow in the chromatographic monolith exists.

References

1. E.F. Hilder, F. Svec, and J.M.J. Frechet. Development and application of polymeric monolithic stationary phases for capillary electrochromatography. *J. Chromatogr. A* **1044:** 3–22 (2004).
2. A.I. Liapis and B.A. Grimes. The effect of the pore structure and zeta potential of porous polymer monoliths on separation performance in ion-exchange mode. *J. Sep. Sci.* **30:** 648–657 (2007).
3. A.I. Liapis and B.A. Grimes. On film mass transfer coefficient expression in ion-exchange chromatography systems. *Separation and Purification Technology* **59:** 342–345 (2008).
4. H. Berg, H. Hansson, and L. Kagedal. U.S. Patent 6,428,707 B1 (2002).
5. B.-L. Johansson, M. Belew, S. Eriksson, G. Glad, O. Lind, J.-L. Maloisel, and N. Norman. Preparation and characterization of prototypes for multi-modal separation media aimed for capture of negatively charged biomolecules at high-salt conditions. *J. Chromatogr. A* **1016:** 21–33 (2003).
6. B.-L. Johansson, M. Belew, S. Eriksson, G. Glad, O. Lind, J.-L. Maloisel, and N. Norman. Preparation and characterization of prototypes for multi-modal separation media aimed for capture of positively charged biomolecules at high-salt conditions. *J. Chromatogr. A* **1016:** 35–49 (2003).
7. X. Zhang, J.-C. Wang, K.M. Lacki, and A.I. Liapis. Construction by molecular dynamics modeling and simulations of the porous structures formed by dextran polymer chains attached on the surface of the pores of a base matrix: characterization of porous structures. *J. Phys. Chem. B* **109:** 21028–21039 (2005).
8. X. Zhang, J.-C. Wang, K.M. Lacki, and A.I. Liapis. Molecular dynamics simulation studies of the conformation and lateral mobility of a charged adsorbate biomolecule: implications for estimating the critical value of the radius of a pore in porous media. *J. Colloid Interface Sci.* **290:** 373–382 (2005).
9 . A.I. Liapis and B.A. Grimes. The coupling of the electrostatic potential with the transport and adsorption mechanisms in ion-exchange chromatography systems: theory and experiments. *J. Sep. Sci.* **28:** 1909–1926 (2005).
10. A. Ljunglöf, K.M. Lacki, J. Mueller, C. Harinarayan, R. Van Reis, R. Fahrner, and J.M. Van Alstine. Ion exchange chromatography of antibody fragments. *Biotechnol. Bioeng.* **96:** 515–524 (2007).
11. E. Riccardi, J.-C. Wang, and A.I. Liapis. Rational surface design for molecular dynamics simulations of porous polymer adsorbent media. *J. Phys. Chem. B* **112:** 7478–7488 (2008).
12. E. Riccardi, J.-C. Wang, and A.I. Liapis. Porous polymer adsorbent media constructed by molecular dynamics modeling and simulations: the immobilization of charged ligands and their effect on pore structure and local nonelectroneutrality. *J. Phys. Chem. B.* **113:** 2317–2327 (2009).
13. B.A. Grimes and A.I. Liapis. The interplay of diffusional and electrophoretic transport mechanisms of charged solutes in the liquid film surrounding charged nonporous adsorbent particles employed in finite bath adsorption systems. *J. Colloid Interface Sci.* **248:** 504–520 (2002).
14. X. Zhang, B.A. Grimes, J.-C. Wang, K.M. Lacki, and A.I. Liapis. Analysis and parametric sensitivity of the behavior of overshoots in the concentration of a charged adsorbate in the adsorbed phase of charged adsorbent particles: practical implications for separations of charged solutes. *J. Colloid Interface Sci.* **273:** 22–38 (2004).
15. X. Zhang, J.-C. Wang, K.M. Lacki, and A.I. Liapis. Molecular dynamics simulation studies of the transport and adsorption of a charged macromolecule onto a charged adsorbent solid surface immersed in an electrolytic solution. *J. Colloid Interface Sci.* **277:** 483–498 (2004).
16. M.P. Allen and D.J. Tildesley. *Computer Simulation of Liquids.* Clarendon Press, Oxford, U.K., 1987.
17. V. Molinero and W.A. Goddard III. M3B: a coarse grain force field for the simulation of oligosaccharides and their water mixtures. *J. Phys. Chem. B* **108:** 1414–1427 (2004).
18. I.G. Tironi, R. Sperb, P.E. Smith, and W.F. van Gunsteren. A generalized reaction field method for molecular dynamics simulations. *J. Chem. Phys.* **102:** 5451–5459 (1995).

Manuscript received December 5, 2008.